AD_____

Award Number: W81XWH-04-1-0262

TITLE: Targeting MRS-Defined Dominant Intraprostatic Lesions with Inverse-Planned High Dose Rate Brachytherapy

PRINCIPAL INVESTIGATOR: Jean Pouliot, Ph.D.

CONTRACTING ORGANIZATION: University of California San Francisco
San Francisco, CA 94143

REPORT DATE: February 2006

TYPE OF REPORT: Annual

PREPARED FOR: U.S. Army Medical Research and Materiel Command
Fort Detrick, Maryland 21702-5012

REPORT DOCUMENTATION PAGE

Form Approved
OMB No. 0704-0188

1. REPORT DATE *(DD-MM-YYYY)*	**2. REPORT TYPE**	**3. DATES COVERED** *(From - To)*
01-02-2006	Annual	26 Jan 2005 - 25 Jan 2006

4. TITLE AND SUBTITLE
Targeting MRS-defined dominant intraprostatic lesions with inverse-planned high dose rate brachytherapy

5a. CONTRACT NUMBER

5b. GRANT NUMBER
W81XWH-04-1-0262

5c. PROGRAM ELEMENT NUMBER

6. AUTHOR(S)
Jean Pouliot, Ph.D.

E-Mail: POULIOT@RADONC17.UCSF.EDU

5d. PROJECT NUMBER

5e. TASK NUMBER

5f. WORK UNIT NUMBER

7. PERFORMING ORGANIZATION NAME(S) AND ADDRESS(ES)

University of California San Francisco
San Francisco, CA 94143

8. PERFORMING ORGANIZATION REPORT NUMBER

9. SPONSORING / MONITORING AGENCY NAME(S) AND ADDRESS(ES)
U.S. Army Medical Research and Materiel Command
Fort Detrick, Maryland 21702-5012

10. SPONSOR/MONITOR'S ACRONYM(S)

11. SPONSOR/MONITOR'S REPORT NUMBER(S)

12. DISTRIBUTION / AVAILABILITY STATEMENT
Approved for Public Release; Distribution Unlimited

13. SUPPLEMENTARY NOTES

14. ABSTRACT:

During this second year, we have obtained CHR approval (December 2004)from the three step process (G.U., P.R.C. and C.H.R.) committees at UCSF. Patient enrollment will begin immediately after receiving CHR approval from D.O.D. We have developed a deformable image registration method to improve the quality of registration of (probe-in) MRSI data for (probe-out) radiation treatment planning. A similarity index (SI) of 98.1 % was obtained for rigid probe patient data. We have also obtained a class solution for the boost of DIL defined by MRI/ MRSI, as well as for the sparing of organs at risk including bladder, rectum, urethra and penile bulb.

15. SUBJECT TERMS
Magnetic resonance spectroscopy, Inverse planning HDR Brachytherapy

16. SECURITY CLASSIFICATION OF:			**17. LIMITATION OF ABSTRACT**	**18. NUMBER OF PAGES**	**19a. NAME OF RESPONSIBLE PERSON**
a. REPORT	**b. ABSTRACT**	**c. THIS PAGE**			USAMRMC
U	U	U	UU	26	**19b. TELEPHONE NUMBER** *(include area code)*

Standard Form 298 (Rev. 8-98)
Prescribed by ANSI Std. Z39.18

Table of Contents

INTRODUCTION

Research Project Description

Recent developments in high spatial resolution Magnetic Resonance Imaging (MRI) and Magnetic Resonance Spectroscopic Imaging (MRSI) from UCSF have significantly improved the ability to identify regions of cancer within the prostate and to discriminate them from surrounding healthy tissues.

In this project, we propose a comprehensive, innovative approach that incorporates MRI / MRSI anatomic and metabolic information to guide the determination of the optimal dose distribution. First, in order to increase radiation to the tumor part of the prostate and to reduce radiation to normal structures, these regions must be reliably identified and delineated in the anatomical image used for the treatment plan. Second, determining such an individualized, complex, conformal radiation dose plan necessitates the use of an optimization algorithm.

Incorporating the MRI/MRSI information is currently difficult. The exam cannot be obtained at the time of the treatment planning MRI due to the need for an endorectal probe and due to artifacts from the catheters inserted for the treatment. To transfer the information from the MRI/MRSI to the treatment planning MRI, tissue distortions must be corrected and the data aligned.

Additionally, we propose to develop a novel high dose rate brachytherapy (HDR) planning protocol using a computerized optimization algorithm using multiple objectives to provide a boost while preserving nearby healthy tissues.

Three main tasks were identified to fulfill the aims of this project:

Task 1: To determine the need for alignment and to establish alignment methods for MRI/MRSI data to HDR brachytherapy treatment planning MRI and CT images. (Months 1-24).

Task 2: To elaborate class solutions (a set of optimization constraints) appropriate for DIL boosts of the order of 150% of the prescribed dose and protection for the penile bulb and the neuro-vascular bundle valid for 90% of the cases (Months 1-12).

Task 3: To perform feasibility and short-term measures of improved effectiveness and decreased side effects of performing the proposed treatment planning protocol in a small cohort of patients (Months 18-36).

The Information provided in this first annual report supports the following:

Task 1: Months 1-24 Completed, (except for alignment of the non-endorectal MR images to the treatment planning CT, pending patient enrollment)
Task 2: Months 1-12 Completed, (except for the inclusion of neuro-vascular bundles, pending patient enrollment)
Task 3: Months 18-36 Not yet initiated

C.H.R. approval

The PC-030909 grant officially opened on February 2004. A lot of effort and time were devoted by the P.I. and Co-P.I. at applying and obtaining approval from the various committees at UCSF. During the first year, we sequentially applied and successfully received approvals from the UCSF Genito-Urinary Committee (GU, March 2004), the UCSF Protocol Review Committee (PRC, July 7th, 2004), and the UCSF Committee on Human Research (CHR, approval number H11386-24294-01, December 17th, 2004). Immediately after receiving the CHR approval, the complete package was submitted to the DOD CHR for final approval. This approval is pending. Patients enrollment will begin when DOD approval is received and final protocol is reviewed by the UCSH CHR Committee.

Research activities

A number of research activities related to the Tasks described in the Statement of Work of the proposal. In particular, Task 1 has been accomplished and published on the journal “Medical Physics”, and Task 2 has been accomplished and submitted on the journal “Radiotherapy and Oncology”. Specific details on each item are provided in the next section. A Postdoctoral Fellow (Yongbok Kim, Ph.D.) continued to perform the work.

In order to make progress as DOD Human Subjects Research Review Board (HSRRB) approval for the research is pending, we have retrospectively looked at MRI data already acquired and anonymized from a different study. This has allowed us to develop appropriate tools and come up to some conclusions as how to progress when DOD approval comes. Hence, we primarily investigated the class solution for the boost of DIL defined by combined MRI/MRSI obtained prior to patient enrollment.

BODY SECTION

In response to the reviewers’ comments on our paper submitted to the Medical Physics Journal, the data from five additional expandable endorectal coil (ERC) patients were added. Globally, the data of 15 rigid ERC and 10 expandable ERC patients were investigated for the analysis of prostate deformation between ERC probe-in and out study. The paper was published in December 2005 (see appendice). In addition, the 5 rigid and 5 expandable ERC axial MR images between ERC-in and out were anonymized and sent to the research group in the Department of Industrial Engineering and Operations Research, University of California, Berkeley, for the study of image-registration using biochemical modeling and non-linear parameter estimation.

Finally, prior to patient enrollment, the class solution for the boost of DIL defined by combined MRI/MRSI was obtained based on the available data of 15 HDR brachytherapy patients.

Endorectal coil probes for prostate MRI: Assessments of tissue distortions and image alignments

Sagittal and axial T_2 weighted MR images were acquired from 25 patients receiving a combined MR imaging (MRI) /MR spectroscopic imaging (MRSI) staging exam for prostate cancer. Within the same exam, images were acquired using an external pelvic phased array coil both alone and in combination with either an expandable ERC (MedRad, Pittsburgh, PA) or a rigid ERC (USA Instruments, Aurora, OH). Rotations, translations and deformations caused by the ERC were measured and compared. The ability to register images acquired with and without the ERC using a manual rigid-body registration was assessed using a similarity index (SI).

Both ERCs caused the prostate to tilt anteriorly with an average tilt of 18.5 degrees (17.4 ± 9.9 and 19.5 ± 11.3 degrees, mean ± standard deviation, for expandable and rigid ERC, respectively). However, the expandable coil caused a significantly larger distortion of the prostate as compared to the rigid coil; compressing the prostate in the anterior/posterior direction by 4.1 ± 3.0 mm versus 1.2 ± 2.2 mm (14.5% versus 4.8%) ($p < 0.0001$), and widening the prostate in the right/left direction by 3.8 ± 3.7 mm versus 1.5 ± 3.1 mm (8.3% versus 3.4%) ($p = 0.004$). Additionally, the ability to manually align prostate images acquired with and without ERC was significantly ($p < 0.0001$) better for the rigid coil (SI = 0.941 ± 0.008 versus 0.899± 0.033, for the rigid and expandable coils, respectively). In conclusion, the manual rigid-body alignment of prostate MR images acquired with and without the ERC can be improved through the use of a rigid ERC.

Registration of MR prostate images with biomechanical modeling and nonlinear parameter estimation

To register diagnostic probe-in magnetic resonance (MR) images to therapeutic probe-out MR images for treatment planning, a deformable image registration method is developed based on biomechanical modeling of soft tissues and on estimation of uncertain tissue parameters using nonlinear optimization.

Given 2D manually segmented probe-in and probe-out MR images, a finite element method (FEM) is used to estimate the deformation of the prostate and surrounding tissues due to displacements and forces resulting from the endorectal probe. Since FEM requires tissue stiffness material properties and external force values as input, the method estimates uncertain parameters using nonlinear local optimization.

The registration method is evaluated using MR images from 5 balloon and 5 rigid endorectal probe patient cases. It requires on average 37 seconds of computation time on a 1.6GHz Pentium-M PC. Comparing the prostate outline in deformed probe-out images to corresponding probe-in images, the method obtains a mean similarity index (SI) of 97.5% and 98.1% for the balloon and rigid probe cases, respectively. The FEM method with nonlinear parameter estimation significantly enhances SI value compared with previous methods ($P < 0.05$), in particular, with greater improvement for balloon probe cases where larger tissue deformations occur.

Class solution for Inverse Planning

We developed a class solution in inverse planned HDR brachytherapy for boosting dominant intra-prostatic lesion (DIL) defined by combined MRI/MRSI prior to enrolling patient for clinical investigation of improved effectiveness and decreased side effect of DIL-boost plan.

For 15 patients, a DIL containing at least 3 contiguous MRSI validated cancer voxels was manually contoured on HDR planning axial CT or MR images. A class solution was developed for DIL-boost plan under dosimetric requirement of (i) RTOG-0321 protocol or (ii) relaxed RTOG-0321 protocol. To determine a maximum attainable level of DIL-boost for each patient, five different levels of DIL-boost were considered, at least 110%, 120%, 130%, 140% and 150% of the prescribed dose. The maximum attainable DIL-boost plan was compared with a plan without boost using averaged cumulative DVH of target and DIL. Several dosimetric indices of target and DIL were also reported between two plans.

By using a class solution the dose escalation of DIL was feasible for 11 out of 15 and 14 out of 15 patients under requirement (i) and (ii), respectively. Target dose was slightly increased, while DIL dose was significantly increased with 40% up to 82% of DIL receiving at least 150% of the prescribed dose without any violation of requirement (i) or (ii). With further adjustment of the class solution, at least 150% DIL-boost was allowed for 13 out of 15 and all 15 patients under requirement (i) and (ii), respectively. Using a class solution for inverse planning based on simulated annealing (IPSA), dose escalation of MRI/MRSI defined DIL up to 150% of the prescription dose while complying with RTOG dosimetric requirements is feasible. This HDR brachytherapy approach to dose escalation allows significant dose increase to tumor and minimizes the risk to patient. The class solution for IPSA defined in this study provides an efficient mean to achieve this goal.

KEY RESEARCH ACCOMPLISHMENTS

Endorectal coil probes for prostate MRI: Assessments of tissue distortions and image alignments

- The average 18.5 degree of anterior prostate tilt was introduced due to ERC. The ability to align prostate MR images acquired with and without ERC was significantly improved when rigid ERC was employed (average percent overlap of ROI is 94.0 %). Hence, the alignment of prostate MRI/MRSI data acquired using an ERC with therapeutic planning MR images acquired without an ERC can be improved through the use of a rigid ERC.

.

Registration of MR prostate images with biomechanical modeling and nonlinear parameter estimation

- This deformable image registration method can improve the quality of registration of (probe-in) MRSI data for (probe-out) radiation treatment planning with a mean SI quality of 97.5% for 5 balloon probe patients and 98.1% for 5 rigid probe patients.

Class solution for Inverse Planning

- The class solution was obtained for the DIL-boost as well as the sparing organs at risk , including bladder, rectum, urethra and penile bulb.

REPORTABLE OUTCOMES

Summary of Reportable Outcomes

Task 1: To determine the need for alignment and to establish alignment methods for MRI/MRSI data to HDR brachytherapy treatment planning MRI and CT images. (Months 1-24).

a) To determine the need and accuracy of aligning MRI/MSRI data acquired with an endorectal probe to images acquired without a probe (10 expandable versus15 rigid patient studies)

1. Both ERCs caused the superior portion of the prostate to tilt anteriorly with an average angle of 18.5 degrees. Specifically, the mean angle change between ERC-in and ERC-out was 19.5 degrees for the rigid coil, and 17.4 degrees for the expandable coil.
2. On average the expandable coil caused a significantly larger distortion of the prostate as compared to the rigid coil; compressing the prostate in the A/P direction by 4.1 ± 3.0 mm (mean ± standard deviation) versus 1.2 ± 2.2 mm (14.5% versus 4.8%) ($p < 0.0001$), and widening the prostate in the R/L direction by 3.8 ± 3.7 mm versus 1.5 ± 3.1 mm (8.3% versus 3.4%) ($p = 0.004$).
3. Degree of image registration was improved in the similarity index attained using the rigid coil. Quantitatively, the ability to align prostate images acquired with and without ERC was significantly ($p < 0.0001$) better for the rigid coil (SI = 0.941 ± 0.008, range from 0.925 to 0.952) than for the expandable coil (SI = 0.899 ± 0.033, range from 0.812 to 0.928). In addition, the average difference of SI values calculated by two different observers is 0.0059 with maximum difference of 0.01972. There was no significant difference between the two observers (p-value is 0.3525 using Wilcoxon matched-pairs signed-ranks test) in obtaining SI values using rigid image registration between ERC-in and ERC-out MR images. However, each prostate contour for a prostate is different to a certain extent depending on each observer.

b) To determine the ability and accuracy of the proposed alignment of the non-endorectal MR images from the MRI/MRSI exam to the treatment planning MRI (Months 1-18).

Deformable image registration for 5 rigid and 5 expandable ERC axial MR images between ERC-in and out study using biochemical modeling and non-linear parameter estimation method.

Biomechanical modeling with nonlinear estimation of uncertain tissue parameters can improve the quality of registration of (probe-in) MRSI data for (probe-out) radiation treatment planning. Improvements in image registration quality are greater for balloon probes compared to rigid probes due to the larger tissue deformations that occur with balloon probes. The algorithm achieved a mean SI quality of 97.5% for 5 balloon probe patients and 98.1% for 5 rigid probe patients. The improvement over center-of-mass rigid registration is statistically significant ($P < 0.05$). Our method reduced displacement error between homologous test points in the probe-in and probe-out images by a mean 74.8% to a mean error of 1.95 mm for balloon probe cases and by a mean 70.0% to a mean error of 0.97 mm for rigid probe cases. The method required on average 37 seconds of computation time on a 1.6GHz Pentium-M laptop PC to estimate and compensate for tissue deformations and produce a nonlinear mapping between probe-in and probe-out images.

However, we have to account for the prostate deformation due to catheter implantation in order to use MRI/MRSI exam into real treatment planning MRI. A full 3D deformable image registration model is desirable to use MRI/MRSI information directly into CT or MRI based HDR planning. However, to implement and evaluate this 3D model will require substantial new research that we estimate will require 2 years to complete. Based on the previous study, manual definition of DIL on planning axial CT or MRI is possible at this point based on the MRI/MRSI information with some uncertainty. The error should be reduced if rigid ERC is employed.

c) To determine ability and accuracy of the proposed alignment of the non-endorectal MR images from the MRI/MRSI exam to the treatment planning CT (Months 6-24).

This portion of Task 1 will be initiated when patient enrollment starts.

Task 2: To elaborate class solutions (a set of optimization constraints) appropriate for DIL boosts of the order of 150% of the prescribed dose and protection for the penile bulb and the neuro-vascular bundle valid for 90% of the cases.

We developed a class solution for boosting MRI/MRS defined DIL in inverse planned HDR brachytherapy of the prostate cancer based on 15 patient data, while complying with dosimetric requirement of (i) RTOG-0321 protocol or (ii) relaxed RTOG-0321 protocol.

a) To determine the parameters of the dose constraints for the protection of the penile bulb. Under both of requirement (i) and (ii), the same class solution was acquired for the penile bulb

Table I

Volume		Weighting factor to D_{Min} for its penalty	D_{Min} [%]	D_{Max} [%]	Weighting factor to D_{Max} for its penalty
BULB of PENIS (Organ at risk)	ON	0	0	50	30
	IN	0	0	50	30

b) To determine the ability of IPSA to limit the dose delivered to the neuro-vascular bundles while keeping an adequate coverage of the prostate. The first objective is to limit the dose to the bundles to 90%. Investigation will be required to determine if a lower value can be reached.

We will include the neuro-vascular bundles for the class solution as soon as MRI-based HDR brachytherapy patients are enrolled in the study.

c) To determine the parameters of the class solution that will fulfill the DIL boost and simultaneously protect the additional organs at risk, bulb and neuro-vascular bundles.

The class solution under requirement (i) is the combination of Table II and IV while the class solution under requirement (ii) is the combination of Table III and IV for the DIL-boost as well as the sparing OAR such as bladder, rectum, urethra and penile bulb.

II. Class solution for a plan without boost under dosimetric requirement (i)

Volume		Weighting factor to D_{Min} for its penalty	D_{Min} [%]	D_{Max} [%]	Weighting factor to D_{Max} for its penalty
Prostate (Target)	ON	100	100	150	100
	IN	100	100	150	30
URETHRA (Organ at risk)	ON	100	100	120	30
	IN	100	100	120	30
BLADDER (Organ at risk)	ON	0	0	50	30
	IN	0	0	50	30
RECTUM (Organ at risk)	ON	0	0	50	30
	IN	0	0	50	30
BULB of PENIS (Organ at risk)	ON	0	0	50	30
	IN	0	0	50	30

III. Class solution for a plan without boost under dosimetric requirement (i)

Volume		Weighting factor to D_{Min} for its penalty	D_{Min} [%]	D_{Max} [%]	Weighting factor to D_{Max} for its penalty
Prostate (Target)	ON	100	100	150	100
	IN	100	100	150	30
URETHRA (Organ at risk)	ON	100	100	120	30
	IN	100	100	120	30
BLADDER (Organ at risk)	ON	0	0	75	40
	IN	0	0	75	40
RECTUM (Organ at risk)	ON	0	0	75	40
	IN	0	0	75	40
BULB of PENIS (Organ at risk)	ON	0	0	50	30
	IN	0	0	50	30

IV. Class solution of DIL under dosimetric requirement (i) and (ii)

Volume		Weighting factor to D_{Min} for its penalty	D_{Min} [%]†	D_{Max} [%]	Weighting factor to D_{Max} for its penalty
DIL (Target)	ON	100	Vary	150	30
	IN	100	Vary	150	5

D_{Min} [%]† varies depending upon the level of DIL-boost (110, 120, 130, 140 or 150).

Task 3: To perform feasibility and short-term measures of improved effectiveness and decreased side effects of performing the proposed treatment planning protocol in a small cohort of patients (Months 18-36).

Task 3 will begin as soon as patient enrollment is initiated.

a) Determine how often the treatment planning method meets the goals of the treatment plan (Months 18-30).
b) Determine if rates of impotence, and in particular acute complications, grade 2 urinary and rectal symptoms are decreased with the new treatment planning protocol as compared to historical values for HDR (Months 24-36).
c) Determine if post-treatment PSA levels are lower and decrease more with the new protocol (Months 30-36).

DETAILS OF REPORTABLE OUTCOMES

Task 1: To determine the need for alignment and to establish alignment methods for MRI/MRSI data to HDR brachytherapy treatment planning MRI and CT images. (Months 1-24).

a) To determine the need and accuracy of aligning MRI/MSRI data acquired with an endorectal probe to images acquired without a probe.

15 rigid ERC and 10 expandable ERC patients were investigated for the analysis of prostate deformation between ERC probe-in and out study.

1. Impact of ERC on prostate location

The rotations of the prostate in coronal and axial planes (Rot_{Cor}, Rot_{Axi}) were visually negligible when we compared coronal and axial T2-weight MR image acquired with and without ERC (Fig. 1(A) and 1(B), respectively). The prostate angle (θ, curved dashed arrow) was measured counterclockwise between the prostate S/I axis (PA) and the line perpendicular to the axis of magnet bore (expressed with a dot straight arrow). The prostate angle was 106.1 and 90.2 degrees for (a) and (b), respectively.

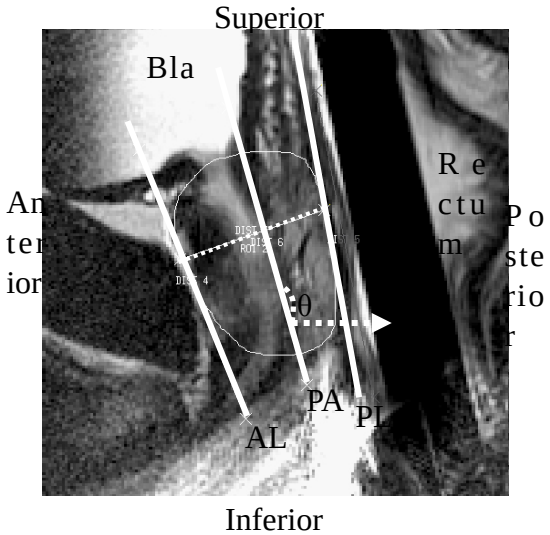

Fig. 1(A)

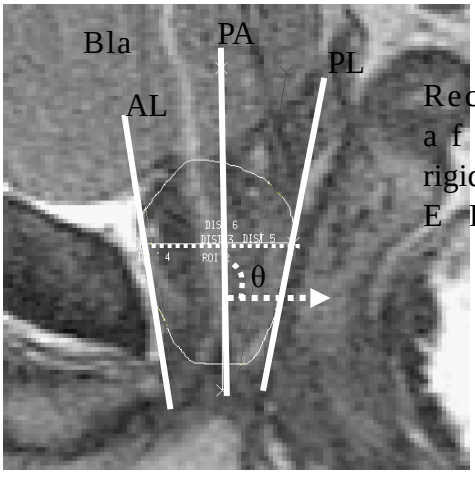

Fig. 1(B)

Figure 2 summarizes the changes in prostate angle between ERC-in and ERC-out studies for the 25 patient studies (15 rigid coil studies, and 10 expandable coil studies. As observed in Figure 1, both ERCs (Fig. 2(A) – rigid coil, Fig. 2(B) – expandable coil) caused the superior portion of the prostate to tilt anteriorly with an average angle of 18.5 degrees. Specifically, the mean angle change between ERC-in and ERC-out was 19.5 degrees for the rigid coil, and 17.4 degrees for the expandable coil.

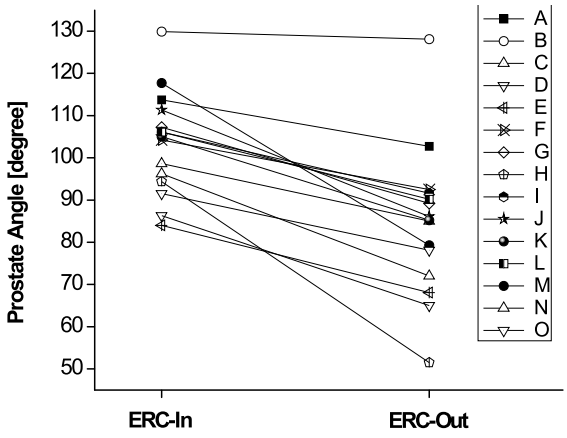

Fig. 2(A)

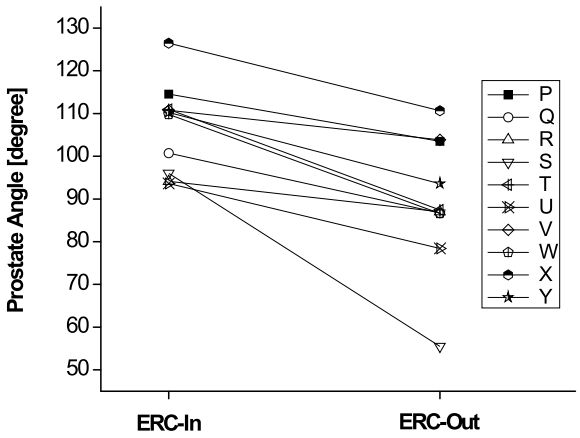

Fig. 2(B)

2. **Impact of ERC on prostate location**

As can be seen in comparing Fig. 1(a) with Fig. 1(b), the presence of the rigid ERC did not affect the S/I length of prostate as compared to the images acquired without the ERC. Quantitatively, the difference in the S/I length of the prostate measured between images acquired with and without either ERC was always less than the thickness of an axial MR image (3 mm).

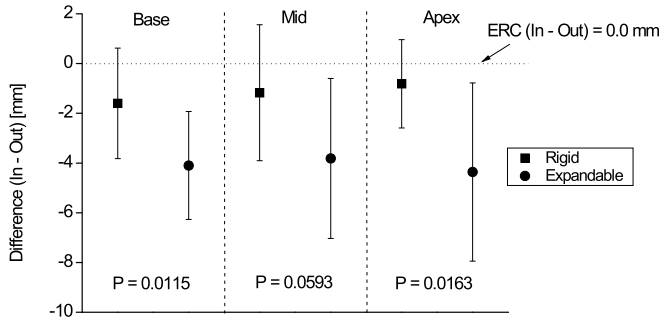

Fig. 3(A)

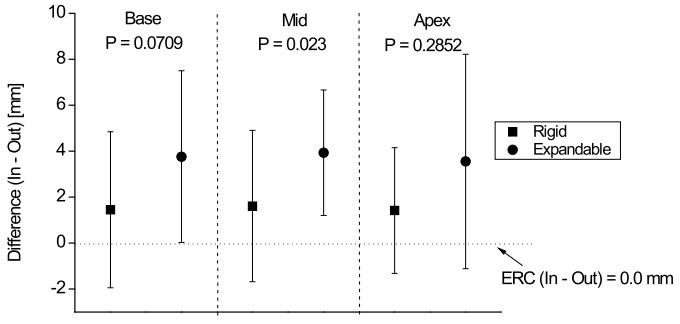

Fig. 3(B)

Figure 3 graphically summarizes the A/P (a) and R/L (b) distortions for the rigid (squares) and expandable (circles) ERCs at the base, midgland and apex of the prostate, with the numerical values reported in Table I. On average the expandable coil caused a significantly larger distortion of the prostate as compared to the rigid coil; compressing the prostate in the A/P direction by 4.1 ± 3.0 mm (mean ± standard deviation) versus 1.2 ± 2.2 mm (14.5% versus 4.8%) ($p < 0.0001$), and widening the prostate in the R/L direction by 3.8 ± 3.7 mm versus 1.5 ± 3.1 mm (8.3% versus 3.4%) ($p = 0.004$). Additionally, the expandable coil consistently caused larger distortions along the S/I length of the prostate (base, midgland and apex of gland) as compared to the rigid coil, with the distortions being significantly larger ($P < 0.05$) at all locations except for the A/P dimension at the midgland and the R/L dimension at the base and apex of prostate due to the large variability of these measurements (Fig. 4(a) and 4(b)). There was no significant difference in the degree of deformation with location (apex, midgland and base) for either ERC.

Table V(A) A/P distance decrease between ERC-in versus ERC-out studies (unit is mm)

S/I Region of Prostate	Type of ERC	Mean (relative change)	Standard Deviation
Base (p= 0.0115)	15 Rigid cases	1.60 (4.9%)	2.22
	10 Expandable cases	4.1 (13.2%)	2.17
Mid (= 0.0593)	15 Rigid cases	1.17 (3.7%)	2.73
	10 Expandable cases	3.82 (13.0%)	3.22
Apex (= 0.0163)	15 Rigid cases	0.81 (3.1%)	1.77
	10 Expandable cases	4.36 (17.2%)	3.58

Table V(B) R/L distance increase between ERC-in versus ERC-out studies (unit is mm)

S/I Region of Prostate	Type of ERC	Mean (relative change)	Standard Deviation
Base (p = 0.0709)	15 Rigid cases	1.45 (4.2%)	3.39
	10 Expandable cases	3.76 (7.7%)	3.74
Mid (p = 0.023)	15 Rigid cases	1.61 (4.3%)	3.29
	10 Expandable cases	3.94 (8.3%)	2.73
Apex (p = 0.2852)	15 Rigid cases	1.42 (4.2%)	2.73
	10 Expandable cases	3.55 (9.0%)	4.66

3. Registration of images acquired with and without ERC

The ability to register images acquired with and without the ERC was determined using a manual rigid-body registration and assessed using a similarity index (SI) [19-20]. Two independent observers did the contouring and registration process for all patients to assess inter-observer differences on the calculated SI. To accomplish this, the contour of the prostate was manually drawn on each contiguous 2-D axial MR image forming a 3-D volume that was aligned between images acquired with and without the ERC. Prior to contouring the prostate, the contiguous 2-D MR images were stacked together to form a 3-D volume, and the volume was rotated in the sagittal plane by the difference in prostate angle after accounting for the series angle (Rot_{sag} = (MRI series angle – prostate angle) $_{ERC\text{-}in}$ – (MRI series angle – prostate angle) $_{ERC\text{-}out}$). Subsequently, the resolution (mm/pixel) of the ERC-in MR images was changed to equal that of the ERC-out MR images and the ERC in and ERC out images were visually aligned in the S/I dimension based on the anatomy of the prostate. Finally, contours were manually drawn on the 2-D images outlining the prostate, and the contoured ERC-in volume was translated in the R/L and A/P directions, based on the mean value of the R/L and A/P coordinates of the contoured ERC-out volume.

The exactness of image registration between ERC in and ERC out contoured volumes was evaluated using a SI value. The SI value (ranging from 0 to 1) was defined as the ratio of twice the common area ($A \cap B$) to the sum of the individual areas ($A + B$). For example, if the

contoured volumes were perfectly matched, the SI value would be 1, whereas no overlap would result in a SI value of 0.

Where ‘A’ and ‘B’ are the two contoured volumes, ‘a’ is the area belonging to only contour volume ‘A’, ‘b’ is the area occupied by only contoured volume ‘B’, and ‘c’ is the overlapping region between volumes ‘A’ and ‘B’.

Figure 4 graphically demonstrates the improvement in the similarity index attained using the rigid coil. Quantitatively, the ability to align prostate images acquired with and without ERC was significantly ($p < 0.0001$) better for the rigid coil (SI = 0.941 ± 0.008, range from 0.925 to 0.952) than for the expandable coil (SI = 0.899 ± 0.033, range from 0.812 to 0.928). In addition, the average difference of SI values calculated by two different observers is 0.0059 with maximum difference of 0.01972. There was no significant difference between the two observers (p-value is 0.3525 using Wilcoxon matched-pairs signed-ranks test) in obtaining SI values using rigid image registration between ERC-in and ERC-out MR images. However, each prostate contour for a prostate is different to a certain extent depending on each observer.

Figure 4.

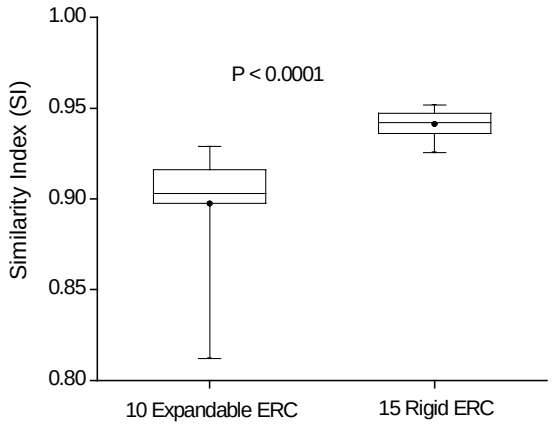

b) To determine the ability and accuracy of the proposed alignment of the non-endorectal MR images from the MRI/MRSI exam to the treatment planning MRI (Months 1-18).

Instead of rigid image registration, deformable image registration using biochemical modeling and non-linear parameter estimation method was performed for 5 rigid and 5 expandable ERC axial MR images between ERC-in and out study.

1. Deformable image registration using 2D finite element method (FEM) with optimized uncertainty parameters.

Our image registration method, which applies to planar slices of tissue, defines a mapping F between a probe-out image and a probe-in image. The mapping F represents the deformation of the prostate and surrounding tissue due to endorectal probe insertion. Given a probe-out image A and a probe-in image B, the goal is to compute F such that $F(A) = B$. The inverse mapping F^{-1}, which can be used during treatment planning, transforms every point in the MRSI grid of the probe-in image B to its coordinate in the probe-out image A.

At the core of our method to compute F is a 2D finite element model that estimates the deformation of soft tissues in the probe-out image due to insertion of the endorectal probe. Treating the uncertain tissue stiffness properties and external forces as unknown variables, we estimate their values using nonlinear local optimization to maximize image registration quality. Our current optimization routine includes 3 uncertain stiffness parameters and between 20 and 40 external forces applied on the prostate boundary, each with 2 degrees of freedom.

The input for our image registration method is a segmented probe-in image and segmented probe-out image. From the probe-in and probe-out MR image volumes, we selected a single probe-in image slice in the mid region of the prostate for each patient. We then manually selected a corresponding probe-out image slice that is at the same level as the probe-in image for the patient. We align rigid points in the images, such as points in bones, using a homologous point method to translate the images.

We manually segmented the selected images using a standard image segmentation method by drawing polygonal outlines on a computer screen to define the boundaries of tissue types. For cases in which the tissue type (such as the rectum) was close to circular, we specified a circle and radius that the software automatically converted to a polygonal approximation. The image registration method requires segmentation of the probe and prostate in the probe-in image and the probe entry location (rectum) and prostate in the probe-out image. For improved accuracy in the biomechanical simulation, we also segmented bones and separately segmented the central gland (CG) and peripheral zone (PZ) of the prostate in the probe-out image. Additional segmentation of the probe-in image will not improve results since the biomechanical model is applied to deform the probe-out image.

The mean SI of our method was 97.5% with a standard deviation of 0.7% for the 5 balloon probe cases. For the 5 rigid probe cases, the mean SI was 98.1% with a standard deviation of 0.4%. As shown for a patient case in Fig. 5, the deformed probe-out image closely matches the probe-in image. In Table VI, we compare our image registration method to rigid registration based on center of mass translation for the prostate total gland. We performed paired *t*-tests to determine the statistical significance ($P < 0.05$) of the results and found that the improvement in SI using our method was statistically significant for both the balloon probe ($P = 0.035$) and the rigid probe ($P = 0.013$) cases.

Figure 5

Table VI. mean and standard deviation (in parentheses) of similarity index (SI) for image registration quality.

	Rigid Translation	Our Method
5 balloon probe cases	86.6% (10.4%)	97.5% (0.7%)
5 rigid probe cases	94.1% (2.7%)	98.1% (0.4%)

$$SI = \frac{2\{A \cap B\}}{A + B} = \frac{2c}{a + b + 2c}$$

The results of our method for the point error metric are shown in Table VII. Our method reduces displacement error between the homologous points in the probe-in and probe-out images by a mean of 74.8% to a mean error of 1.95 mm for the balloon probe cases. For the rigid probe cases, the reduction was by a mean of 70.0% to a mean error of 0.97 mm. We performed paired *t*-tests and found that the reduction in error was statistically significant for both the balloon probe ($P = 0.0045$) and the rigid probe ($P = 0.0099$) cases.

Table VII. Point displacement error means and standard deviations (in parentheses) for a sample homologous point on the boundary of the prostate central gland and peripheral zone near the midline.

	Mean point error for probe-in / probe-out images (mm)	Mean point error after our method (mm)	Mean reduction in error (%)
5 balloon probe cases	9.22 (3.22)	1.95 (0.22)	74.8% (15.1%)
5 rigid probe cases	3.93 (1.59)	0.97 (0.51)	70.0% (27.2%)

2. **Warping the MRSI grid.**

The 3D MRSI data is collected from a volume and individual spectra are generally reconstructed for 7 x 7 x 7 mm^3 voxels within a grid overlaid on this volume. To help register spectroscopic data to the probe-out image, we transform each intersection point in the regular MRSI grid from the probe-in image plane to the probe-out image using the inverse of mapping *F*. The warped MRSI grid is the output of the algorithm: it registers the probe-in MRSI data to probe-out image for use during treatment planning.

We show the output of our image registration method for a sample balloon probe patient in Fig. 6 and for a rigid probe patient in Fig. 7. The resulting warping of the MRSI grid is clearly nonlinear in both cases. The percentage of strain energy due to external forces *E* averaged 8.6% for balloon probe cases and 10.0% for rigid probe cases. The low value for *E* demonstrates that, for both types of probes, most of the strain energy in the finite element simulation was due directly to the displacement of tissues caused by the probe rather than other uncertain external forces. Mean computation time for the image registration algorithm was comparable for both balloon and rigid probe patients on a 1.6GHz Pentium-M laptop PC: 39.8 seconds with a standard deviation of 20.8 seconds for balloon probe cases and 34.2 seconds with a standard deviation of 11.8 seconds for rigid probe cases.

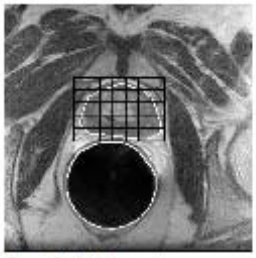

Fig. 6 (a) Input: Given probe-in image *B* with MRSI grid

Fig. 6 (b) Intermediate step: Deformed probe-out image *F*(*A*) with MRSI grid

Fig. 6 (c) Output: Given probe-out image *A* with warped MRSI grid

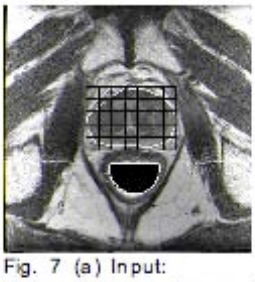

Fig. 7 (a) Input: Given probe-in image *B* with MRSI grid

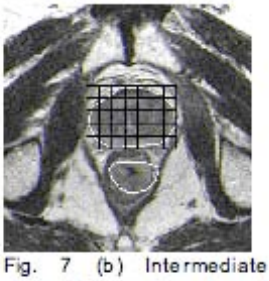

Fig. 7 (b) Intermediate step: Deformed probe-out image *F*(*A*) with MRSI grid

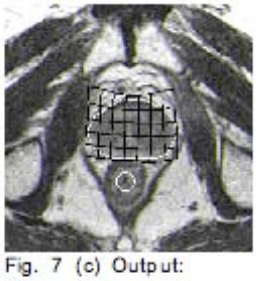

Fig. 7 (c) Output: Given probe-out image *A* with warped MRSI grid

Our current method independently registers 2D slices of tissue from a 3D MRI volume. We are currently developing an analogous 3D biomechanical simulation and image registration method to explicitly account for deformations and displacements that occur between imaging planes in 3D volumes. Generating patient-specific 3D conformal tetrahedral meshes with a controlled number of elements and validating the 3D image registration approach using a new imaging protocol with slices sufficiently thin to capture out-of-plane deformations will require substantial new research. We also plan to extend the method to register deformations that occur due to catheter insertion for HDR brachytherapy treatment planning, which will also require a new imaging data set and new models of forces exerted by the catheters on soft tissue.

However, we have to account for the prostate deformation due to catheter implantation in order to use MRI/MRSI exam into real treatment planning MRI. A full 3D deformable image registration model is desirable to use MRI/MRSI information directly into CT or MRI based HDR planning. However, to implement and evaluate this 3D model will require substantial new research that we estimate will require 2 years to complete. Based on the previous study, manual definition of DIL on planning axial CT or MRI is possible at this point based on the MRI/MRSI information with some uncertainty. The error should be reduced if rigid ERC is employed.

c) To determine ability and accuracy of the proposed alignment of the non-endorectal MR images from the MRI/MRSI exam to the treatment planning CT (Months 6-24).

Task 2: To elaborate class solutions (a set of optimization constraints) appropriate for DIL boosts of the order of 150% of the prescribed dose and protection for the penile bulb and the neuro-vascular bundle valid for 90% of the cases.

We developed a class solution for boosting MRI/MRS defined DIL in inverse planned HDR brachytherapy of the prostate cancer.

Combined MRI/MRSI and Definition of DIL

Combined MRI/MRSI information to identify DIL in the prostate was available for 15 HDR patients (later referred to as patients A to O). The information was clinically used in HDR brachytherapy treatment planning for 4 prostate cancer patients while retrospectively used for 11 patients after HDR brachytherapy treatment. The mean ± standard deviation value of prostate volume is 43.7 ± 16.3 cc with a range from 28.1 to 86.0 cc. In general, 16 catheters (range from 15 to 18) were inserted under transrectal ultrasound (TRUS) guidance to cover the entire target volume. Two fractional HDR with an interstitial was delivered over two days with 9.5Gy of prescribed dose (total of 19Gy). The mean ± standard deviation value of DIL volume in percent relative to prostate volume is 13.9 ± 7.3% with a range from 2.5 to 31.3% for 15 patients. All patients have one DIL except for patient J who has two DILs. In this study DIL is always located at the peripheral zone of prostate and its specific location is different depending on each patient: right side, left side or midline in the peripheral zone of prostate when seen in axial planning CT or MR image. For example, a DIL is delineated at the right side in the peripheral zone of prostate in axial CT image (Fig. 8 (b)) for HDR prostate brachytherapy planning since a validated cancer lesion comprises five contiguous voxels with a score of 5 (definitively abnormal) at the same location of prostate shown in the combined axial MRI/MRSI image (Fig. 8 (a)). Each MRSI voxel is scored using a standardized 5-point scale (1- definitely benign, 2- likely benign, 3- equivocal, 4- likely abnormal and 5- definitely abnormal), based on the change of metabolite markers (choline, citrate, creatine and polyamines): elevation of choline peak and reduction of citrate and creatine peaks in an abnormal MRSI voxel. Based on the combined MRI/MRSI information, DILs were manually contoured on HDR planning axial CT or MR images. A lesion was defined as a DIL (Fig. 8 (B)) wherever it contains at least 3 contiguous MRSI validated cancer voxels scored with 4 or 5 in combined MRI/MRSI images (Fig. 8 (A)).

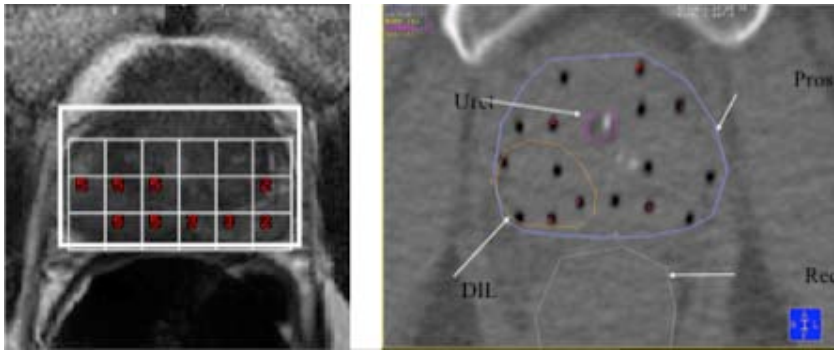

Figure 8

Dosimetric requirements for class solution

Two different sets of dosimetric requirements were employed to develop a class solution (i) RTOG (Radiation Therapy Oncology Group) 0321 protocol (Phase II trial of combined high dose rate brachytherapy and external beam radiotherapy for adenocarcinoma of the prostate) requires more than 90% of target coverage (V100[%] > 90%) and less than 1 cc of dose to OAR such as bladder, rectum and urethra (V75[cc] < 1 cc for bladder and rectum, V125[cc] < 1 cc for urethra). To provide more possibility of dose escalation on DIL while keeping more than 90% of target coverage, the dose limit to bladder and rectum in RTOG-0321 dosimetric requirement was relaxed up to 2 cc (V75[cc] < 2 cc for bladder and rectum) instead of 1 cc. In this study it is named as (ii) relaxed RTOG-0321 dosimetric requirement. Throughout the paper, target V100[%] is defined as the percent volume [%] of target receiving at least 100% of the prescribed dose while rectum V75[cc] is defined as the absolute volume [cc] of rectum receiving at least 75% of the prescribed dose. The name of anatomy and its numeric value vary for the specific interest.

Class solution for a plan without boost

An inverse planning routine based on simulated annealing algorithm (IPSA) was developed and a beta version of the IPSA algorithm was implemented on the commercial HDR treatment planning system (Plato V14.2, Nucletron, The Netherlands) for evaluation and clinically/routinely used for the HDR brachytherapy in our institute. First of all, in axial CT or MR images the anatomy of target and OAR is delineated and catheters are digitized. On the surface and inside of all organs (targets and OAR), a set of dose constraints is defined: acceptable dose range (minimum and maximum doses) and weighting factors for penalty values imposed to minimum and maximum doses. Under those user-defined dose constraints, IPSA searches the optimal solution (a dwell time distribution for possible source dwell positions along the catheters) within a minute.

Prior to developing a class solution for DIL-boost plan, a class solution for a plan without boost was determined. Based on our previous clinical experience in IPSA for HDR prostate brachytherapy, dose constraint for target and urethra are well established and clinically/routinely used in our institute. In general, acceptable dose range is always the same both on the surface and inside of all organs (targets and OAR). The clinically acceptable dose range is from 100% to 150% of the prescribed dose for target and from 100% to 120% for urethra, which has to be spared from high dose (hot spot). To other OAR located outside of the target such as bladder and rectum, ideally no dose should be delivered. Hence, naught is assigned to minimum dose while clinically appropriate value such as 50% or 75% of the prescribed dose with its pertinent weighting factor to maximum dose. For weighting factors to the dose limit, both on the surface and inside of the OAR the same value was applied because any dose should be avoided both on the surface and inside of the OAR simultaneously. However, they were different between on the surface and inside of the target. On the surface of the target, they should be high (such as 100) enough to ensure the clinically acceptable target coverage by the prescribed dose and the avoidance of any

dose beyond the target volume to protect OAR adjacent to the target. Inside the target, weighting factor to minimum dose was also high enough (such as 100) that the inside of target is fully covered by the prescribed dose whereas weighting factor to maximum dose was relaxed (30 is used in our institute) to achieve better conformal dose distribution within the target. Since catheters are located in the target, high dose more than 150% of the prescribed dose is inevitable. However, still hot spot should be avoided in some degree. For urethra the same weighting factors as the inside of target are used based on the previous clinical experience. Regarding weighting factors to dose limit of bladder and rectum, they are well established but sometimes vary depending on individual patient in order to yield a clinically better plan, a better tradeoff between higher target coverage by the prescribed dose and enhanced protection of bladder and rectum. Therefore, if the maximum dose limit of bladder and rectum is decreased and/or their weighting factor is increased unduly, rectum and bladder are overprotected with losing target coverage reluctantly. On the other hand, if their maximum dose is increased and/or their weighting factor is reduced excessively, the target coverage with the prescribed dose can be improved but rectum and bladder receive intolerable dose and consequently higher complication is predictable after treatment. Therefore, in this study, by adjusting the maximum dose and weighting factor of bladder and rectum a class solution was determined for a plan without boost under either dosimetric requirement (i) or (ii). In this study, 9 out of 15 patients have the contour of bulb of penis and the class solution for bulb of penis was obtained with the same way for bladder and rectum. For all the patients, no dose is delivered to the bulb of penis at V50[cc] under requirement (i) and (ii), respectively.

Table VIII(a) and VIII(b) are class solutions developed for a plan without boost under requirement (i) and (ii), respectively. All plans employing the class solution, Table VIII(a), satisfied all dosimetric requirements (i) with mean target coverage of 92.4% (range from 90 to 94.7%), except for 3 patients (B, J, L). For those patients, maximum dose and/or its weighting factor for bladder and rectum were tuned to meet requirement (i). In contrast, all plans employing the class solution, Table IX(b), satisfied all dosimetric requirements (ii) with mean target coverage of 95.3% (range from 92.9 to 96.9%). Thanks to the relaxation of dose limit to bladder and rectum, target coverage under requirement (ii) is improved by 2.9% compared with that under requirement (i) and no further adjustment of the class solution is necessary to satisfy requirement (ii) for all patients.

Table VIII(a) Class solution for a plan without boost under dosimetric requirement (i)

Volume		Weighting factor to D_{Min} for its penalty	D_{Min} [%]	D_{Max} [%]	Weighting factor to D_{Max} for its penalty
Prostate (Target)	ON	100	100	150	100
	IN	100	100	150	30
URETHRA (Organ at risk)	ON	100	100	120	30
	IN	100	100	120	30
BLADDER (Organ at risk)	ON	0	0*	50	30
	IN	0	0*	50	30
RECTUM (Organ at risk)	ON	0	0*	50	30
	IN	0	0*	50	30
BULB of PENIS (Organ at risk)	ON	0	0*	50	30
	IN	0	0*	50	30

Abbreviations applied to Table VIII and IX
ON: on the surface of the contour; IN: inside the volume
D_{Min} [%] and D_{Max} [%]: Minimum and maximum dose in percent with respect to the prescribed dose, respectively.
0*: any number is acceptable for the minimum dose since weighting factor is null.

Table VIII(b) Class solution for a plan without boost under dosimetric requirement (ii)

Volume		Weighting factor to D_{Min} for its penalty	D_{Min} [%]	D_{Max} [%]	Weighting factor to D_{Max} for its penalty
Prostate (Target)	ON	100	100	150	100
	IN	100	100	150	30
URETHRA (Organ at risk)	ON	100	100	120	30
	IN	100	100	120	30
BLADDER (Organ at risk)	ON	0	0*	75	40
	IN	0	0*	75	40
RECTUM (Organ at risk)	ON	0	0*	75	40
	IN	0	0*	75	40
BULB of PENIS (Organ at risk)	ON	0	0*	50	30
	IN	0	0*	50	30

Class solution for DIL

A class solution of DIL was developed based on three perspectives. Primarily the dosimetric requirement (i) or (ii) should be constantly satisfied while a class solution was investigated. Second, in the literature there is no data available for the clinically acceptable level of DIL-boost in HDR prostate brachytherapy. In this study the maximum dose to the target (150% of the prescribed dose) was conservatively used as an objective dosimetric index to be maximized for DIL-boost plan. At last, the 150% of the prescribed dose was also utilized as maximum dose limit of DIL in order to avoid excessive increase of DIL volume in the dose range of more than 150% of the prescribed dose even though DIL was identified as the validated cancer lesion inside the prostate.

Prior to examining various levels of DIL-boost for each patient, the same dose range as target was applied for DIL to construct a DIL-boost plan equivalent to a plan without boost. As with target and OAR, the same dose range was used both on the surface and inside of the DIL. On the surface of DIL the same weighting factors as the inside the target were employed because theDIL surface has the same clinical importance as the inside of target. In addition, the weighting factor for the minimum dose inside the DIL was the same value as inside the target since the DIL should be covered by at least minimum dose. Finally, for appropriate weighting factor to the maximum dose limit inside the DIL, seven different values of weighting factor (from 0 to 30 with 5 points increment) were attempted in the DIL-boost plan equivalent to a plan without boost under either dosimetric requirement (i) or (ii).

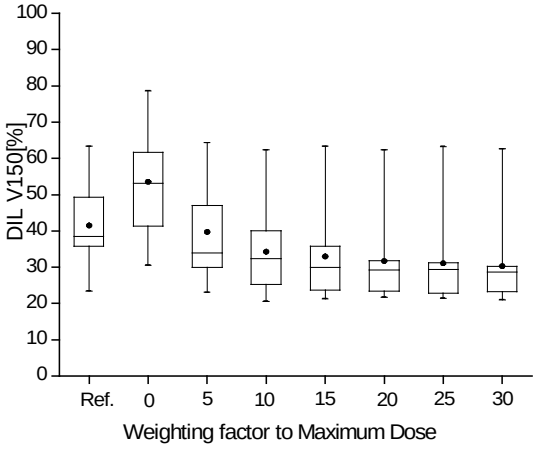

Fig. 9 (a)

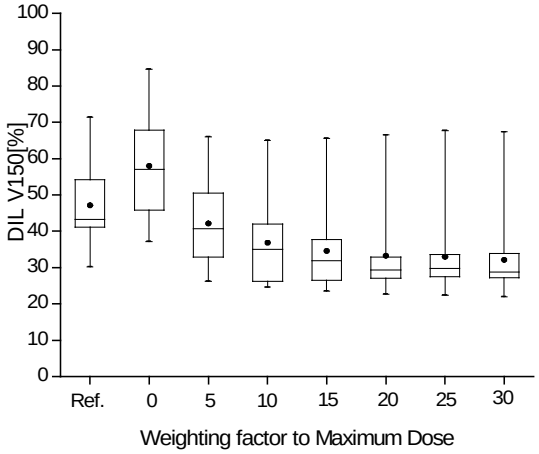

Fig. 9(b)

Table IX Class solution of DIL under dosimetric requirement (i) and (ii)

Volume		Weighting factor to D_{Min} for its penalty	D_{Min} [%]†	D_{Max} [%]	Weighting factor to D_{Max} for its penalty
DIL (Target)	ON	100	Vary	150	30
	IN	100	Vary	150	5

D_{Min} [%]† varies depending upon the level of DIL-boost (110, 120, 130, 140 or 150).

Maximum attainable level of DIL-boost using the class solution

The class solution for DIL-boost plan was developed by adding a dose constraint for the DIL to the previously obtained class solution for a plan without boost. By increasing minimum dose with 10 points increment in the class solution for the DIL-boost plan equivalent to a plan without boost, five different level of DIL-boost plans were investigated for each patient: 110 – 150, 120 – 150, 130 – 150, 140 – 150, and 150 – 150 (acceptable dose range: minimum – maximum dose in percent relative to the prescribed dose). The highest DIL-boost plan without any violation of requirement (i) or (ii) was considered as the maximum attainable DIL-boost plan for each patient. For patients who allowed a certain level of DIL-boost, the maximum attainable DIL-boost plan was compared with a plan without boost by analyzing cumulative dose volume histogram (DVH) of target and DIL. Additionally, specific dosimetric indices of target (V100[%] and V150[%]) and DIL (V120[%], V150[%] and V200[%]) were compared between two plans. Furthermore, under requirement (i) or (ii) the class solution was manually adjusted to achieve the 150 – 150 DIL-boost for those patients who previously prohibited that boost. One out of seven weighting factors to the maximum dose was chosen based on three perspectives previously mentioned in the Methods and Materials section and a class solution of DIL for the same level of DIL-boost as target was constructed under requirement (i) or (ii). As the weighting factor applied to the maximum dose is increased, the value of DIL V150[%] is reduced due to the heavily imposed penalty value to the maximum dose for both cases (i) and (ii) in Fig 9.

In case of no penalty value (zero weighting factor) applied, much higher dose can be delivered to DIL (V150[%] value is improved in Fig. 9, but DIL volume in the dose range of more than 150% of the prescribed is also undesirably increased). If rectum and/or bladder is very closely located to the DIL, dosimetric requirement would be violated: in this study, patients B, E and J violated bladder dose limit and patients B, F and O violated rectum dose limit under requirement (i) while patient J violated bladder dose limit under requirement (ii). For six non-zero different weighting factors applied to maximum dose, the degree of protection of OAR was the same: rectum dose limit was violated for patients F and O and bladder dose limit was violated for patient J under requirement (i) while all requirements (ii) were satisfied. Without any benefit in the protection of OAR the higher weighting factor deteriorated DIL V150[%] value (Fig. 9). Therefore, the value of 5 was chosen as the best weighting factor in both cases (i) and (ii) and the class solution of DIL were achieved on the surface and inside of the DIL (Table 2) for DIL-boost study.

The class solution obtained by combining a class solution for without-boost plan (Table 1) and a class solution of DIL (Table 2) was exploited to acquire the maximum attainable level of DIL-boost for each patient. Under dosimetric requirement (i), four (B, F, J, O) out of 15 patients prohibited any DIL-boost whereas a certain level of DIL-boost was feasible for the remaining 11 patients (Fig. 10(a)). By averaging all target and DIL DVHs of those patients, a mean DVH was generated for target (Fig. 10(b)) and DIL (Fig. 10(e)) between plan without boost and maximum attainable DIL-boost plan. The averaged target DVHs between two plans were almost the same up to 100% of the prescribed dose and they slightly differed in the rest of the dose range (Fig. 10(b)). In particular, target coverage by the prescribed dose (Fig. 10(c)) was insignificantly increased merely by 1.1%, on average, because the prostate was already satisfactorily covered by the prescribed

dose (92%) prior to DIL-boost and target V150[%] was increased by 6%. On the contrary, the averaged DIL DVH of maximum attainable DIL-boost plan was noticeably shifted into higher dose range (from dash line (N) to dot line (B) in Fig. 10(e)) due to DIL-boost with a maximum increase of 41.8% at the 150% of the prescribed dose (Max.(B-M) of solid line (B-M) in Fig. 10(e)). The significant improved dosimetric indices were observed for all 11 patients (on average, V120[%] was increased from 83.6% to 99% in Fig. 10(f), V150[%] was from 40.6% to 82.4% in Fig. 10(g), and V200[%] was from 13.2% to 33.2% in Fig. 10(h)). As far as the prevention of 150 – 150 DIL-boost is concerned, eight patients did not allow that boost (Fig. 10(a)), in particular no boost for 4 patients and lower level of DIL-boost for the other 4 patients. Out of those 8 patients, patient J and L violated the bladder dose limit while the rest of six patients rectal dose limit under requirement (i). The 150 – 150 DIL-boost could not be accomplished in case deficient number of catheters was implanted to cover the whole prostate and/or rectum and/or bladder was located very close to the target. For example, the volume of prostate B is 86 cc (the largest prostate in this study) and the number of catheters employed is 17. To make matters worse, one of 17 catheters was implanted outside of the target and rectum is located highly close to prostate. Therefore, prostate B prohibited the 150 – 150 DIL-boost under dosimetric requirement (i) despite manual adjustment of the class solution. For patient J, the size of prostate (51.3 cc) is just larger than average and 18 catheters were well implanted to cover the entire prostate. However, both rectum and bladder are located extremely close to the target and the rectal and bladder dose limit of dosimetric requirement (i) were violated for 150 – 150 DIL-boost even though the class solution was manually adjusted.

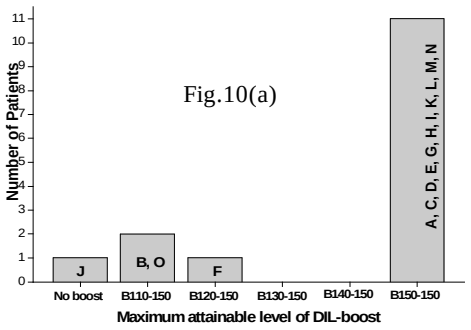

Fig.10(a)

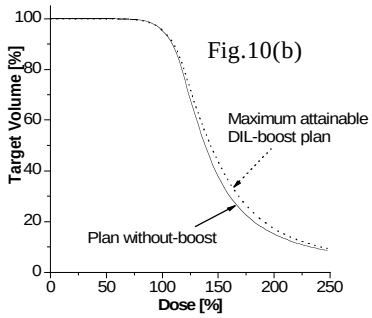

Fig.10(b)

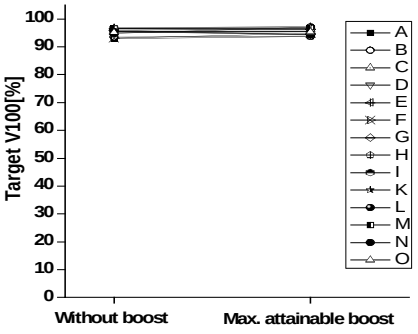

Fig.10(c)

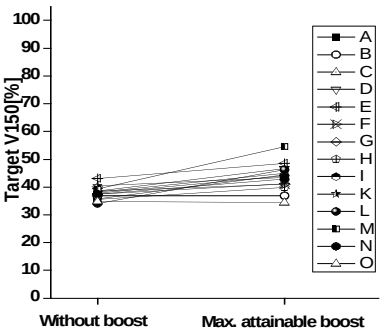

Fig.10(d)

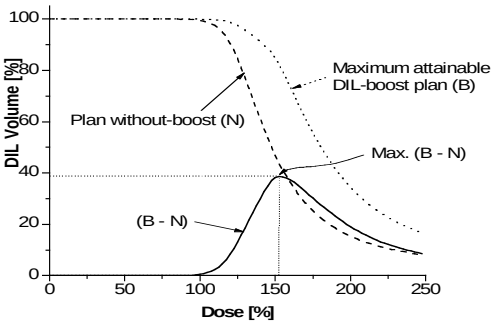

Fig.10(e)

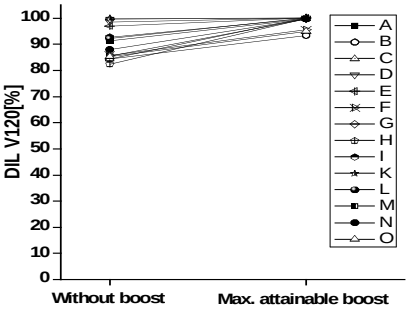

Fig.10(f)

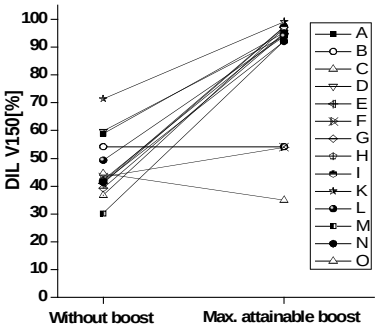

Fig.10(g)

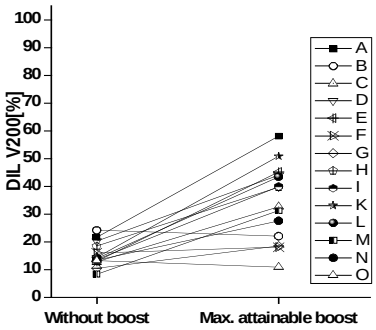

Fig.10(h)

Under dosimetric requirement (ii), a certain level of DIL-boost was accomplished for all patients except for patient J (Fig. 11(a)) using the class solution for a DIL-boost plan. The averaged target and DIL DVH between plan without boost and maximum achievable DIL-boost plan are shown in Fig. 11(b) and 11(e), respectively. The same trend of target and DIL DVH was observed as under requirement (i): target DVHs (Fig. 11(b)) between two plans were slightly different (V100[%] was approximately identical, 95.3% versus 95.5%, on average, in Fig. 11(c) and V150[%] were slightly increased by average 5.8% due to DIL-boost in Fig. 11(d)) while DIL DVHs (Fig. 11(e)) between two plans were considerably different (on average, V120[%] was raised up to 98.8% from 90.5% in Fig. 11(f), V150[%] was extremely elevated from 46.8% to 85.1% in Fig. 11(g), and V200[%] was from 15.4% to 34.5% in Fig. 11(h)). The proximity of OAR adjacent to the prostate prohibited 150 – 150 DIL-boost under requirement (ii). Four patients forbid 150 – 150 DIL-boost in Fig. 4(a) because patient J received overdose on bladder while the other 3 patients on rectum.

Under dosimetric requirement (i) and (ii), in most patients the DIL-boost increased the DIL dose compared with plan without boost in Figs. 10 and 11. However, in Fig. 10(h) DIL V200[%] was decreased for patient H (from 14.3 to 14.0%). In Figs. 11(g) and 11(h), DIL V150[%] and V200[%] were reduced for patient B (from 54.3 to 54.2% and from 24.3 to 22.1%, respectively) and O (from 44.6 to 35.0% and from 13.3 to 11.0%, respectively) despite DIL-boost. For those patients, the maximum attainable level of DIL-boost is not sufficiently high (110% of the prescribed dose as shown in Figs. 10(a) and 11(a)). Such an insufficient DIL-boost in conjunction with dosimetric requirement on OAR, sometimes, may cause the decreased DIL V150[%] and V200[%] during redistribution of hot spot in the prostate.

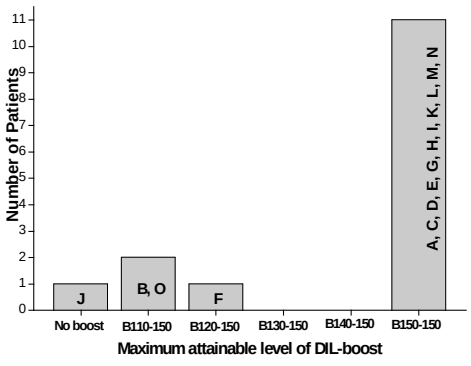

Fig.11(a)

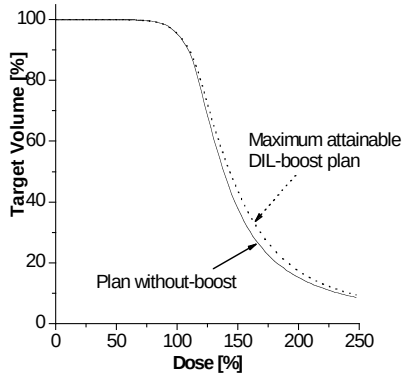

Fig.11(b)

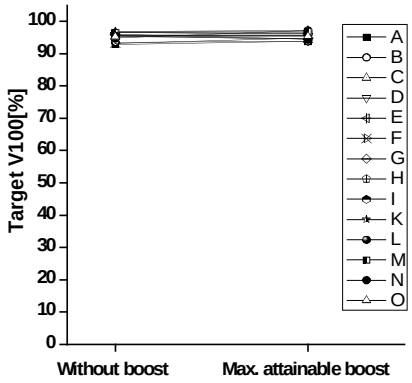

Fig.11(c)

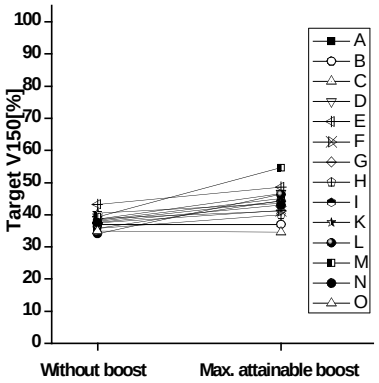

Fig.11(d)

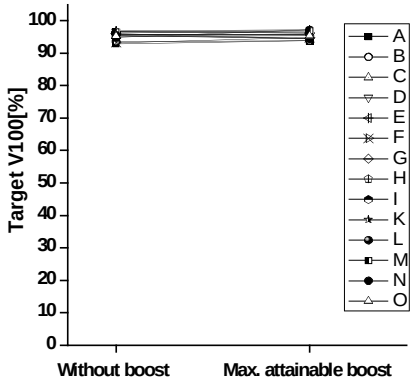

Fig.11(c)

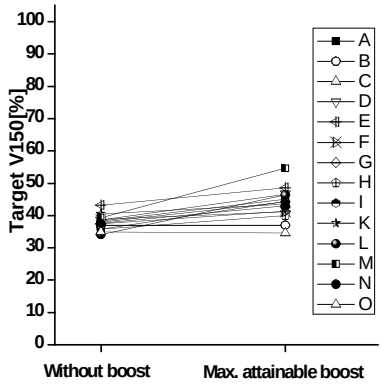

Fig.11(d)

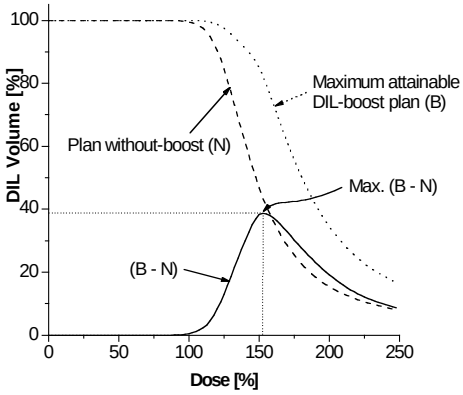

Fig.11(e)

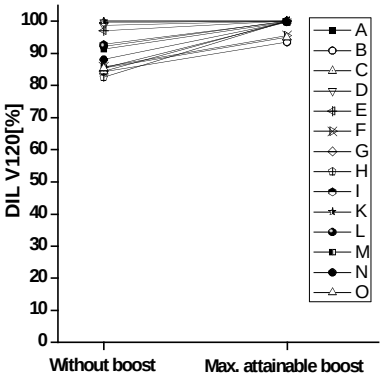

Fig.11(f)

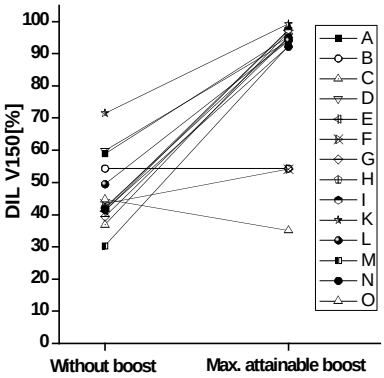

Fig.11(g)

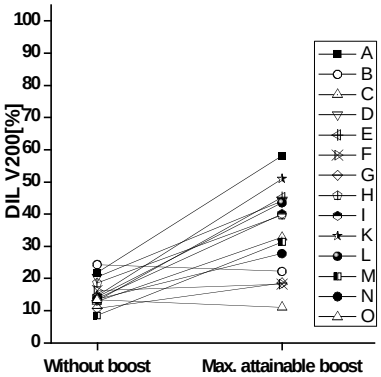

Fig.11(h)

Additionally, by small manual adjustment of a class solution 150 – 150 DIL-boost was fulfilled without any violation of requirement (i) and (ii) for 6 out of 8 patients (except for patient B and J) and all 4 patients (B, F, J, O) who previously offended requirement (i) and (ii), respectively.

The dosimetric requirement of RTOG-0321 protocol is, in some degree, stringent to be accomplished. More patients prohibited 150 – 150 DIL-boost under RTOG-0321 requirement compared with relaxed requirement (8 out of 15 versus 4 out of 15). In particular, satisfying the rectal dose limit (V75[cc] < 1 cc) deteriorated the target coverage (V100[%] < 90%) for patient B and J despite manual adjustment of a class solution to achieve 150 – 150 DIL-boost.

In this study the 150% of the prescribed dose was used for both minimum and maximum dose limit of DIL which means to boost DIL with as least 150% of the prescribed dose as well as to prevent excessive high dose (more than 150% of the prescribed dose) within DIL simultaneously. This purpose was moderately feasible by relaxing weighting factor applied to the maximum dose of the inside of DIL with the value of 5 instead of 30 applied on the surface of DIL and inside the target. As seen a solid line in Fig. 10(e) and Fig. 11(e), the increase of DIL volume due to DIL-boost has the maximum value at the vicinity of 150% of the prescribed dose: on average, 41.8% increase from 40.6% to 82.4% at the 150% of the prescribed dose under requirement (i) and 38.8% increase from 43.7% to 82.5% at the 152.5% of the prescribed dose under requirement (ii), respectively. This can be interpreted that the most sensitive dose of DIL to dose escalation using the class solution obtained in this study was the 150% of the prescribed dose.

d) To determine the parameters of the dose constraints for the protection of the penile bulb.

The answer was displayed in Table 1 above.

e) To determine the ability of IPSA to limit the dose delivered to the neuro-vascular bundles while keeping an adequate coverage of the prostate. The first objective is to limit the dose to the bundles to 90%. Investigation will be required to determine if a lower value can be reached.

We will include the neuro-vascular bundles for the class solution as soon as MRI-based HDR brachytherapy patients are enrolled.

f) To determine the parameters of the class solution that will fulfill the DIL boost and simultaneously protect the additional organs at risk, bulb and neuro-vascular bundles.

The answer was the combining the previously mentioned Table 1 and 2.

Task 3: To perform feasibility and short-term measures of improved effectiveness and decreased side effects of performing the proposed treatment planning protocol in a small cohort of patients. (Months 18-36).

Task 3 will begin as soon as patient enrollment is initiated.

LIST OF ACRONYMS

CHR: Committee on Human Research
CT: Computed Tomography
DIL: Dominant Intraprostatic Lesion
S/I: Superior-Inferior
R/L: Right-Left
A/P: Antero-Posterior
DOD: Department of Defense
ERC: Endo-Rectal Coil
GU: Genito-Urinary Committee
HDR: High Dose Rate
IPSA: Inverse Planning with Simulated Annealing
MRI: Magnetic Resonance Imaging
MRSI: Magnetic Resonance Spectroscopy Imaging
PRC: Protocol Review Committee
ROI: Region of Interest
RTOG: Radiation Therapy Oncology Group
SI: Similarity Index
UCSF: University of California, San Francisco
Vn[%]: Percentage of Volume Receiving n% of the Prescribed Dose
Vn[cc]: Volume in Cubic Centimeter Receiving n% of the Prescribed Dose
DIL Dominant Intra-prostatic Lesion
2D/3D 2 Dimension/3 Dimension
CG Central Gland
PZ Peripheral Zone
FEM Finite Element Method
TRUS Trans-Rectal Ultra-Sound
OAR Organs at Risk

APPENDICE

Publications

1- Kim Y., Noworolski S.M., Pouliot J., Hsu I.C. and Kurhanewicz J., **Endorectal and rigid coils for prostate MRI: Impact on prostate distortion and rigid image registration**, Med. Phys. 32 (12); 3569-3578, 2005.

2- Kim Y., Hsu I.C., Lessard E., Kurhanewicz J.,, Noworolski S.M. and Pouliot J., **Class solution in inverse planned HDR prostate brachytherapy for dose escalation of DIL defined by combined MRI/MRSI**, in Preparation, to be submitted to Int. J. Radiation Onc. Biol. Phys. 2006.

3. Alterovitz R., Goldberg K., Pouliot J., Hsu I.C., Kim Y., Noworolski S.M., and Kurhanewicz J., Registration of MR prostate images with biomechanical modeling and nonlinear parameter estimation, Med. Phys. 33(2), 446-454; 2006. (related to present work but not supported by DOP).